Improved target stability using picket pulses to increase and shape the ablator adiabat[a)]

J. P. Knauer,[b)] K. Anderson, R. Betti, T. J. B. Collins, V. N. Goncharov, P. W. McKenty, D. D. Meyerhofer, P. B. Radha, S. P. Regan, T. C. Sangster, and V. A. Smalyuk
Laboratory for Laser Energetics, University of Rochester, Rochester, New York 14623

J. A. Frenje, C. K. Li, R. D. Petrasso, and F. H. Séguin
Plasma Science Fusion Center, Massachusetts Institute of Technology, Cambridge, Massachusetts 02139

(Received 19 November 2004; accepted 31 January 2005; published online 15 April 2005)

Hydrodynamic simulations have shown that a picket pulse preceding the main target drive pulse in a direct-drive inertial confinement fusion implosion can reduce both the ablation-interface Rayleigh–Taylor (RT) seed and growth rate by increasing the adiabat (ratio of the plasma pressure to the Fermi-degenerate pressure) while maintaining the low adiabat in the inner-fuel layer for optimal target compression and a minimal drive energy for ignition. Experiments with planar and spherical targets have been carried out on the OMEGA [T. R. Boehly, D. L. Brown, R. S. Craxton, R. L. Keck, J. P. Knauer, J. H. Kelly, T. J. Kessler, S. A. Kumpan, S. J. Loucks, S. A. Letzring, F. J. Marshall, R. L. McCrory, S. F. B. Morse, W. Seka, J. M. Soures, and C. P. Verdon, Opt. Commun. **133**, 495 (1997)] laser system, showing that the RT growth of nonuniformities was reduced by picket-pulse laser illumination. Adiabat shaping in spherical targets has been investigated with two types of picket pulses—a "decaying shock wave" and a "relaxation" picket. Planar growth measurements using a wide, intense picket to raise the adiabat of a CH foil showed that the growth of short-wavelength perturbations was reduced, and even stabilized, by adjusting the intensity of the picket. Planar imprint experiments showed the expected reduction of imprinting when a picket pulse is used. The data show that the imprint level was reduced when a picket was added and for short wavelengths was as effective as one-dimensional (1D), 1.5 Å smoothing by spectral dispersion. A series of implosion experiments with a 130 ps wide picket pulse showed a clear improvement in the performance of direct-drive implosions when the picket pulse was added to the drive pulse. Results from relaxation-picket implosions show larger yields from fusion reactions when the picket drive was used. These adiabat-shaping concepts make the likelihood of achieving ignition with direct-drive implosions on the National Ignition Facility [W. S. Hogan *et al.*, Nucl. Fusion **41**, 567 (2001)] significantly more probable. © *2005 American Institute of Physics*.
[DOI: 10.1063/1.1882332]

I. INTRODUCTION

The minimum energy required for ignition of the imploding capsule in inertial confinement fusion[1] is a strong function of the fuel adiabat α_{stag} (the ratio of the shell pressure to the Fermi-degenerate pressure) at the time of maximum compression: $E_{\min} \sim \alpha_{\mathrm{stag}}^{1.9}$.[2,3] The shell must be driven on the lowest possible adiabat to minimize this energy. The performance of low-adiabat implosions is limited by hydrodynamic instabilities that tend to disrupt the shell during the acceleration phase. The most important instability is the Rayleigh–Taylor (RT) (Refs. 4 and 5) instability that is seeded by single-beam nonuniformities and surface roughness. The RT growth is reduced by mass ablation from the target surface,[6–9] characterized by the ablation velocity V_a.

Interface perturbations grow exponentially ($a = a_0 e^{\gamma t}$) during the "linear" phase of RT instability and reach a saturation phase (when $a \sim \lambda/10$) where the growth continues at a reduced rate.[10] Here, a is the amplitude of the perturbation, a_0 is the initial perturbation amplitude (the seed), γ is the growth rate, and λ is the wavelength of the perturbation.

A great deal of effort has gone into reducing the seeds a_0 caused by illumination nonuniformities (imprinting) and target imperfections. The effect of imprinting has been reduced by the number of beam-smoothing techniques, including distributed phase plates (DPPs),[11] polarization smoothing (PS) with birefringent wedges,[12] smoothing by spectral dispersion (SSD),[13] and induced spatial incoherence.[14] The effect of RT instability can also be reduced by lowering the RT growth rate. Theoretical work that includes the effect of thermal transport[9] shows that the RT-growth-rate dispersion formula for a DT target is given by

$$\gamma_{\mathrm{DT}} = \sqrt{A_T(L_0,\nu)kg - A_T^2(L_0,\nu)k^2 V_a V_{\mathrm{bo}}} - [1 + A_T(L_0,\nu)]kV_a,$$

where $A_T(L_0,\nu)$ is the Atwood number (a function of L_0 and ν), k is the perturbation spatial wave number, g is the acceleration, L_0 is the ablation-interface thickness, V_a is the ablation velocity, V_{bo} is the "blowoff" velocity, and ν is the ther-

[a)]Paper BI2 3, Bull. Am. Phys. Soc. **49**, 23 (2004).
[b)]Invited speaker.

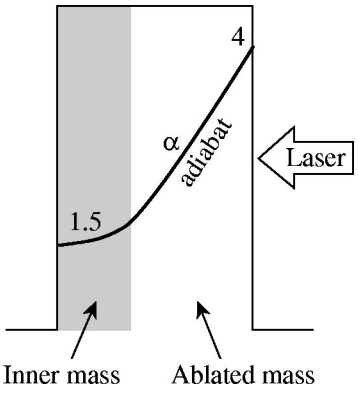

FIG. 1. Schematic of a shell showing a shaped adiabat between the ablation surface and the inner surface. The shaded region is the portion of the shell that is not ablated. The adiabat is higher in the ablated material and therefore reduces the RT growth of ablation-interface perturbations.

mal transport index. V_{bo} is equal to V_a times the ratio of the blowoff plasma density to the ablation-surface density. The ablation velocity, in turn, increases with the adiabat α in the ablation region as $V_a \propto \alpha^{3/5}$ (Ref. 15). This is the compromise that target designers face: lowering α reduces the minimum energy required for ignition, but increases the effects of RT instability. This paper describes recent results using a shaped adiabat that increases the ablation-surface adiabat while maintaining a low adiabat for the compressed fuel.

II. ADIABAT SHAPING

The conflicting requirements of the lower-adiabat fuel at the maximum compression and the higher-adiabat ablation region can be achieved by shaping the adiabat inside the shell. A schematic of a shaped shell adiabat is shown in Fig. 1, where the shell is represented as a region of constant density and the adiabat varies from 1.5 to 4. The shaded region is the portion of the shell that remains at the end of the acceleration phase of the implosion. The inner-fuel region is on a low adiabat, while the adiabat in the ablated mass is high. The first published work on adiabat shaping used the absorption of low-energy x rays[16] to increase the adiabat at the ablation surface.

A short, high-intensity picket pulse, as seen in Fig. 2(a), can be used to shape the shell adiabat by creating a decaying shock wave.[17,18] This technique modifies the adiabat by modifying the pressure inside the shell. The ablation pressure from the picket pulse creates a shock wave that raises the pressure at the ablation surface and propagates into the shell. A rarefaction wave propagates toward the shock wave at the end of the picket pulse. The shock-wave pressure then decays after the rarefaction wave overtakes it, reducing the pressure and lowering the adiabat for the inner sections of the shell.

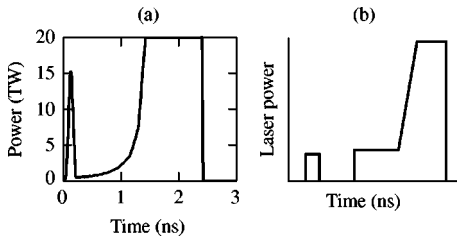

FIG. 2. Laser pulse shapes for a decaying-shock-wave picket and a relaxation picket. (a) The decaying shock wave is created by the short picket at the beginning of the pulse shape. The adiabat is shaped as the shock wave decays. Figure (b) shows the pulse shape for a relaxation-picket drive. The low-intensity, narrow picket in front creates a spatial density profile that is low at the ablation region and high inside the shell. The strong shock wave resulting from the high foot intensity then propagates through this density profile shaping the shell adiabat.

The shell adiabat can also be shaped by propagating a strong shock wave in a fluid where the density increases from the ablation surface to the inner shell.[19] This density shape is created by a low-intensity, narrow picket pulse that causes the shell to decompress after it is turned off, shown in Fig. 2(b). Shell decompression creates a density profile that is low at the ablation interface and high in the inner shell. The pulse shape needs to be timed so that the shock wave from the drive pulse reaches the shell-gas interface at the same time as the rarefaction wave from the picket pulse.

The Laboratory for Laser Energetics (LLE) has done planar RT growth experiments,[20] planar imprint reduction, and spherical implosions with picket pulses. An analytical understanding of adiabat shaping with picket pulses has been established.[17–19] The results from these early experiments and our analytical understanding of picket pulses are being used to improve direct-drive target performance.

III. PLANAR EXPERIMENTS

Acceleration interface perturbation growth due to the RT instability has been routinely studied in planar targets. A nonconverging, planar target allows the whole foil to be placed on a high adiabat to study how the adiabat affects the RT growth. The mass-modulated accelerated foil was composed of a 20 μm thick CH foil with perturbations imposed on the side irradiated by the laser.[21] The initial perturbations have (1) a wavelength of $\lambda = 60$ μm and amplitude $a = 0.25$ μm; (2) $\lambda = 30$ μm and $a = 0.125$ and 0.25 μm; and (3) $\lambda = 20$ μm and $a = 0.05$ and 0.25 μm. The perturbation amplitudes decreased with decreasing wavelength to ensure that the growth was measured in the linear ($a < \lambda/10$) phase of the RT instability. The 0.25 μm amplitude perturbation at wavelengths of 30 μm and 20 μm was used to study the stability of this perturbation for large picket intensities where little or no growth was expected and the smaller amplitude perturbation was below the detection threshold. These targets were accelerated using ten laser beams overlapped with a total peak intensity of 1.7×10^{14} W/cm^2. The use of DPPs, PS, and SSD resulted in a laser-irradiation nonuniformity relative to the intensity envelope of $<1\%$ over a 600 μm diameter region defined by the 90% intensity contour. Two pulse shapes were used for the drive beams: first, a pulse with a Gaussian rise to a 2 ns constant intensity (referred to as the drive pulse) and, second, this same pulse with a Gaussian picket placed ~2 ns ahead of the time when the drive pulse reaches constant intensity, shown in Fig. 3(a). The maximum drive intensity was designed to be the same for irradiation with and without a picket.

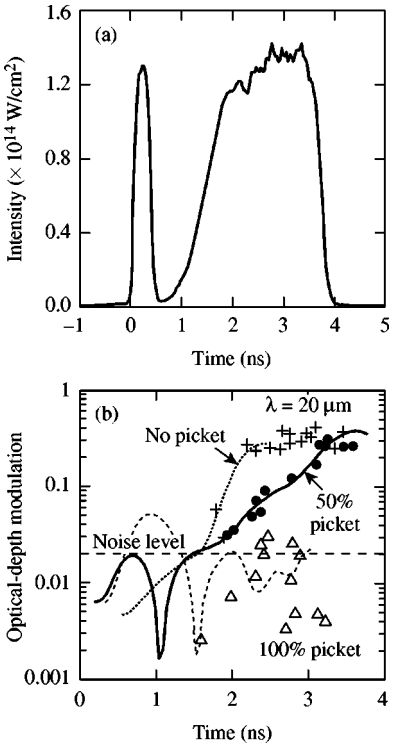

FIG. 3. Planar RT growth experiments used the pulse shape shown in (a). The 300 ps wide picket caused the foil to decompress, lowering the ablation-interface density and raising the ablation velocity. The modulation in optical depth is shown in (b) for an imposed 20 μm wavelength perturbation. Plus signs represent data without a picket, solid circles represent data for a picket with an intensity of 50% of the drive, and open triangles represent data for a picket with an intensity of 100% of the drive. Dotted (no picket), solid (50% picket), and dashed (100% picket) lines show 2D hydrodynamic simulations of the experiments. The noise level of the measurement is shown as the horizontal dashed line.

The calculated and measured amplitudes of the fundamental Fourier mode of the optical-depth modulation for a 20 μm wavelength perturbation are compared in Fig. 3(b) for a drive pulse only, a picket 50% of the drive-pulse intensity, and a picket 100% of the drive intensity. The data with and without the picket have been temporally shifted to match the start of the measured drive pulse. Multiple shots were performed at each wavelength with the x-ray diagnostics using different temporal windows covering the duration of the drive pulse. A clear reduction in the 20 μm wavelength perturbation growth rate is seen for the 50% I_p/I_d data. Data for a picket with an intensity of 100% of drive pulse show that the ablation velocity during the drive pulse is large enough to stabilize the RT growth at this wavelength. Two-dimensional (2D) hydrodynamic simulations of the experiment are plotted as a dotted line (no picket), a solid line (50% picket), and a dashed line (100% picket). The calculated optical-depth modulation agrees with the experimental data in all cases. Both the experimental data and the 2D simulation of the optical depth for the 100% intensity picket pulse remain below or close to the instrumental noise.

A picket pulse is also effective in reducing the imprint seed for the RT instability in cryogenic implosions.[22] Current cryogenic targets are thin (~3–5 μm) CH shells with a 100 μm layer of DT or D_2 ice. The density mismatch between the

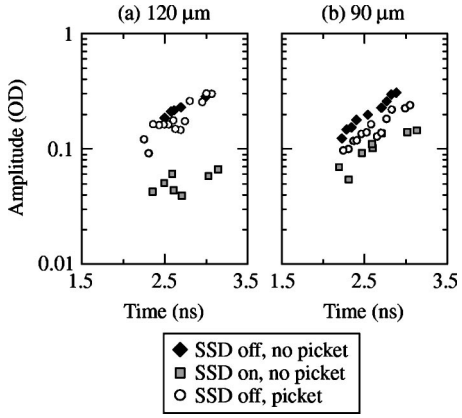

FIG. 4. Imprinting data for 120 μm and 90 μm intensity perturbations. Data with SSD off and no picket are plotted as solid diamonds. Data with SSD off and with the picket are plotted as circles. Data for 1D, 1.5 Å SSD without the picket are shown as open squares.

CH shell and the hydrogenic layer causes a pressure gradient to be established during the constant-intensity foot portion of the laser illumination. The ablation surface is accelerated as a result of the pressure gradient, and the laser imprint is amplified by the RT instability. A picket pulse mitigates the pressure gradient and reduces the RT amplification of the laser nonuniformities and thus reduces the RT seed from imprinting for the target implosion.

Planar experiments were done to study imprint reduction with picket pulses for layered targets. The planar targets were constructed with a 5 μm thick, solid-density CH layer and a 90 μm thick CH foam layer with a density of 0.18 g/cm^3. This foil target acts as a surrogate for a section of a cryogenic spherical target. Intensity perturbations with wavelengths of 120, 90, 60, and 30 μm using specifically designed DPPs in a single beam were imposed on these planar foils. Figures 4 and 5 show the experimental optical-depth-modulation amplitude for these perturbations. Data in Figs. 4(a) and 4(b) show little reduction in the imprinting for long-wavelength perturbations when the picket pulse was used. There is no difference at 120 μm wavelength perturba-

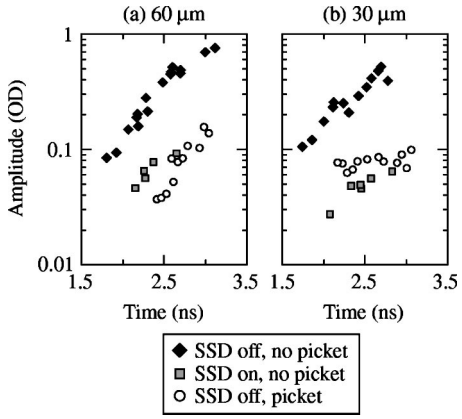

FIG. 5. Imprinting data for 60 μm and 30 μm intensity perturbations. Data with SSD off and no picket are plotted as solid diamonds. Data with SSD off and with the picket are plotted as circles. Data for 1D, 1.5 Å SSD without the picket are shown as open squares.

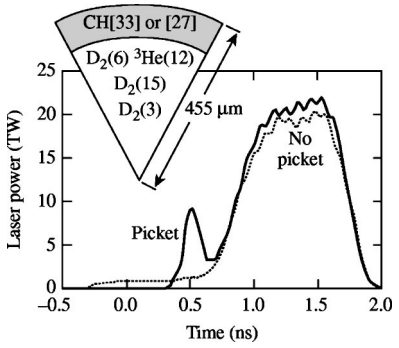

FIG. 6. Pulse shapes used for decaying-shock-wave picket-pulse experiments. The picket drive is shown as the solid curve and the no-picket drive as the dotted curve. The targets used are shown as an inset. The shell thickness in microns is noted by brackets and the gas pressure in atmospheres by parentheses.

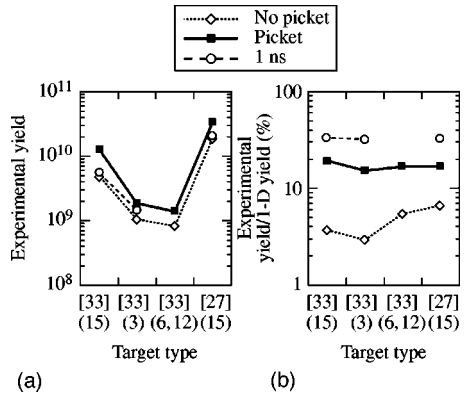

FIG. 7. DD fusion neutron yield from the decaying-shock-wave picket-pulse implosions. The absolute yields are shown in (a) and the normalized yields in (b). The picket data are plotted as the solid squares, nonpicket data are plotted as open diamonds, and 1 ns, square-pulse implosions are plotted as open circles.

tions [Fig. 4(a)] with and without the picket. The data for a 90 μm wavelength perturbation [Fig. 4(b)] and with the picket pulse lie between the data without the picket and with SSD off and SSD on. The shorter-wavelength perturbations show a greater effect on optical-depth modulation for the picket pulse [Figs. 5(a) and 5(b)].

Modulation in optical-depth data shows that the amplitude of the imprint with the picket is the same as that when SSD is on and there is no-picket pulse. The DPPs used to impose the intensity perturbations are refractive optics, so SSD will not affect the perturbation wavelength but will reduce the contrast and thus, the perturbation amplitude. The picket is as effective as 1D, 1.5 Å SSD at reducing the imprint for 60 μm wavelength [Fig. 5(a)] and 30 μm wavelength [Fig. 5(b)] perturbations.

The temporal evolution of the optical-depth data shown in Figs. 4 and 5 show that only the 30 μm wavelength perturbation has its RT growth rate reduced. This is not unexpected. Previous planar growth experiments with picket pulses[20] have shown that the RT growth of long-wavelength perturbations ($\lambda \geqslant 60\ \mu$m) is less affected by the picket pulse than the short-wavelength perturbations ($\lambda = 30$ and 20 μm). This is a result of the k dependence of the ablation-velocity stabilization term in the dispersion formula for the RT growth rate.

IV. SPHERICAL EXPERIMENTS

The OMEGA (Ref. 23) laser system imploded spherical targets with the pulse shapes shown in Fig. 6. The targets used for these measurements are shown as the inset in Fig. 6. The shells were made of either 33 or 27 μm thick polystyrene and filled with three gas-fill conditions: 15 atm of D_2; 3 atm of D_2; and a mixture of 12 atm of ^{3}He and 6 atm of D_2. The target diameters ranged from 901 to 923 μm.

Results from the DD fusion neutron measurements for three shots for each target and pulse shape are shown in Figs. 7(a) and 7(b). For the 15 atm D_2-filled, 33 μm thick shell [Fig. 7(a)], there is a factor of 3 increase in the number of D_2 neutrons from the target irradiated with a picket pulse than that from the target without a picket. The experiment was optimized for the 33 μm thick shells; the improvement for the 27 μm thick shells is only 50%. Both the 3 atm D_2-filled and the ^{3}He–D_2-filled, 33 μm thick shells show an improved fusion yield by a factor of 2. The ratio of the measured primary neutron yield to the neutron yield predicted by the one-dimensional (1D) hydrodynamics simulation [usually referred to as yield-over-clean (YOC)] is plotted in Fig. 7(b) and shows that the 15 atm D_2-filled, 33 μm thick shell improves from 0.03 to 0.19. In all cases, the YOC can be seen to improve significantly. The results from high-adiabat implosions with 1 ns square drive pulses are also plotted in Figs. 7(a) and 7(b). The absolute fusion yield from the 1 ns square data is between yields measured without the picket and with the picket pulse. A high-adiabat implosion will have a lower calculated yield, and therefore the YOC data for the 1 ns^2 implosions are higher than either the nonpicket or picket YOCs. Measurements were made for both the DT and D^{3}He secondary reactions for D_2-filled targets and the D^{3}He primary reaction in the D^{3}He-filled targets. There is insufficient space to present these data, but in all cases, the yields were higher for the picket pulse than for the nonpicket-pulse illumination.

The OMEGA laser system was also used to study the effect of relaxation-picket target designs on imploding CH shells. A relaxation-picket implosion uses a picket in front of a drive pulse that has a high foot intensity. The picket is separated from the drive pulse by a region of zero intensity during which time a rarefaction wave causes the shell to decompress. These pulse shapes are shown in Fig. 8. The picket pulse had a full width at half maximum of ~60 ps. The targets shown schematically by the inset in Fig. 8 were designed for a total laser energy of 18 kJ. They are 870 μm diameter, 35 μm thick CH shells and are filled with 15 atm of D_2.

The measured experimental yields increased when a relaxation (RX) picket pulse was used. The neutron yields shown in Table I were taken for laser drives with and without SSD and with and without a picket pulse. With either SSD on or SSD off, the neutron yields were higher when a picket-pulse drive was used. The yield increased by a factor of 2.5 with SSD off. The laser energy (17.3 ± 0.2 kJ) was very

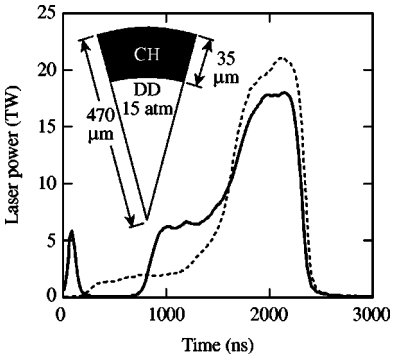

FIG. 8. Pulse shapes used for relaxation-picket-pulse experiments. The picket drive is shown as a solid curve and the no-picket drive as a dashed curve. The targets used are shown in the inset.

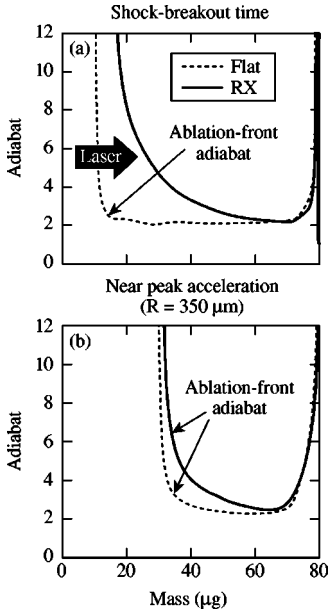

FIG. 9. Shell adiabat shapes for the relaxation-picket drive implosions plotted as a function of Lagrangian mass. Shapes for the start of the acceleration are shown in (a) and those for the peak of the acceleration are shown in (b). The nonpicket drive is shown as a dashed curve while the picket drive profiles are shown as a solid curve.

stable for these implosions, allowing for the direct comparison of measured yield data. The clean 1D hydrodynamics simulation yield with and without the relaxation-picket pulse is also shown in Table I. The simulations show a 25% increase from 4×10^{10} to 5×10^{10} when the relaxation-picket-pulse shape is used.

One-dimensional hydrodynamic simulations[24] were used to calculate the adiabat shapes shown in Fig. 9 at the start of acceleration and at peak acceleration. *LILAC* simulations indicate that RX adiabat shaping in CH is effective throughout the acceleration phase. The adiabat without a picket pulse is illustrated as the "flat" case. At the start of shell acceleration, the adiabat is nearly constant at $\alpha=2$ when no-picket pulse is used. The RX drive has an adiabat of $\alpha=\sim12$ at the ablation interface and an $\alpha=2$ for the inner shell layer. The shape of the adiabat is still steeper for the RX drive at the time of peak acceleration, thus maintaining the effect of a high adiabat at the ablation interface while keeping a low ($\alpha=2$) adiabat in the shell's interior.

V. CONCLUSIONS

Picket pulses coupled to a low-adiabat drive pulse reduce both imprinting and perturbation growth. Adiabat shaping has the potential to improve target stability without significantly increasing the energy needed for compression and ignition. The ablation surface has a high adiabat to increase the ablation velocity and therefore reduce the RT growth. This is done while maintaining the inner portions of the shell on a low adiabat so that the energy needed to compress the core is minimized. The adiabat can be shaped either by launching a decaying shock wave that has a high pressure at the ablation surface and a low pressure at the inner shell surface, or by using a picket pulse to produce a spatial density distribution so that a strong shock wave propagating from the ablation interface to the inner shell surface produces an adiabat that is high in the ablated material and low in the compressed material.

Planar experiments with picket pulses show a reduction in RT growth and imprinting, and spherical experiments with picket pulses show increased fusion yields when a picket pulse is used. With a picket-pulse intensity equal to 50% of the drive-pulse intensity, the RT growth was reduced for a 20 μm wavelength surface perturbation and no significant RT growth was measured for a picket intensity equal to 100% of the drive pulse. Imprint experiments demonstrated that picket pulses were as effective as 1D, 1.5 Å SSD at the reduction of imprint for both 60 μm and 30 μm wavelength perturbations. Spherical target experiments were done with picket pulses that generate a decaying shock wave and a relaxed density profile. The yields of fusion products are improved both in terms of the absolute value and in terms of the comparison to 1D hydrodynamic simulation output for the decaying-shock-wave picket and the absolute yield increased with SSD on and SSD off when the relaxation picket was used.

Results with warm CH targets and calculations with cryogenic targets indicate that picket pulses can be used for NIF direct-drive implosions. Either the decaying-shock-wave

TABLE I. Measured experimental yields increase when a relaxation picket is used.

	SSD off yield ($\times10^9$)	SSD on yield ($\times10^9$)	Clean 1D yield ($\times10^{10}$)
Picket	5.6±0.2	6.8±0.2	5.2±0.5
No picket	2.2±0.1	5.5±0.5	4.0±0.2

or the relaxation-picket-pulse shape can be used to improve the likelihood of achieving ignition.

ACKNOWLEDGMENTS

This work was supported by the U.S. Department of Energy Office of Inertial Confinement Fusion under Cooperative Agreement No. DE-FC52-92SF19460, the University of Rochester, and the New York State Energy Research and Development Authority. The support of DOE does not constitute an endorsement by DOE of the views expressed in this paper.

[1] J. Nuckolls, L. Wood, A. Thiessen, and G. Zimmerman, Nature (London) **239**, 139 (1972).
[2] M. C. Herrmann, M. Tabak, and J. D. Lindl, Nucl. Fusion **41**, 99 (2001).
[3] R. Betti, K. Anderson, V. N. Goncharov, R. L. McCrory, D. D. Meyerhofer, S. Skupsky, and R. P. J. Town, Phys. Plasmas **9**, 2277 (2002).
[4] Lord Rayleigh, Proc. London Math. Soc. **XIV**, 170 (1883).
[5] G. Taylor, Proc. R. Soc. London, Ser. A **201**, 192 (1950).
[6] S. E. Bodner, Phys. Rev. Lett. **33**, 761 (1974).
[7] J. D. Lindl, in *Inertial Confinement Fusion*, edited by A. Caruso and E. Sindoni (Editrice Compositori, Bologna, Italy, 1989), p. 595.
[8] H. Takabe, K. Mima, L. Montierth, and R. L. Morse, Phys. Fluids **28**, 3676 (1985).
[9] R. Betti, V. N. Goncharov, R. L. McCrory, P. Sorotokin, and C. P. Verdon, Phys. Plasmas **3**, 2122 (1996).
[10] S. W. Haan, Phys. Rev. A **39**, 5812 (1989).
[11] T. J. Kessler, Y. Lin, J. J. Armstrong, and B. Velazquez, in *Laser Coherence Control: Technology and Applications*, edited by H. T. Powell and T. J. Kessler (SPIE, Bellingham, WA, 1993), Vol. 1870, p. 95.
[12] T. R. Boehly, V. A. Smalyuk, D. D. Meyerhofer, J. P. Knauer, D. K. Bradley, R. S. Craxton, M. J. Guardalben, S. Skupsky, and T. J. Kessler, J. Appl. Phys. **85**, 3444 (1999).
[13] S. Skupsky, R. W. Short, T. Kessler, R. S. Craxton, S. Letzring, and J. M. Soures, J. Appl. Phys. **66**, 3456 (1989).
[14] R. H. Lehmberg and S. P. Obenschain, Opt. Commun. **46**, 27 (1983).
[15] J. D. Lindl, *Inertial Confinement Fusion: The Quest for Ignition and Energy Gain Using Indirect Drive* (Springer, New York, 1998), Chap. 5, p. 54.
[16] J. H. Gardner, S. E. Bodner, and J. P. Dahlburg, Phys. Fluids B **3**, 1070 (1991).
[17] V. N. Goncharov, J. P. Knauer, P. W. McKenty, P. B. Radha, T. C. Sangster, S. Skupsky, R. Betti, R. L. McCrory, and D. D. Meyerhofer, Phys. Plasmas **10**, 1906 (2003).
[18] K. Anderson and R. Betti, Phys. Plasmas **10**, 4448 (2003).
[19] K. Anderson and R. Betti, Phys. Plasmas **11**, 5 (2004).
[20] T. J. B. Collins, J. P. Knauer, R. Betti, T. R. Boehly, J. A. Delettrez, V. N. Goncharov, D. D. Meyerhofer, P. W. McKenty, S. Skupsky, and R. P. J. Town, Phys. Plasmas **11**, 1569 (2004).
[21] J. P. Knauer, R. Betti, D. K. Bradley, T. R. Boehly, T. J. B. Collins, V. N. Goncharov, P. W. McKenty, D. D. Meyerhofer, V. A. Smalyuk, C. P. Verdon, S. G. Glendinning, D. H. Kalantar, and R. G. Watt, Phys. Plasmas **7**, 338 (2000).
[22] T. J. B. Collins and S. Skupsky, Phys. Plasmas **9**, 275 (2002).
[23] T. R. Boehly, D. L. Brown, R. S. Craxton, R. L. Keck, J. P. Knauer, J. H. Kelly, T. J. Kessler, S. A. Kumpan, S. J. Loucks, S. A. Letzring, F. J. Marshall, R. L. McCrory, S. F. B. Morse, W. Seka, J. M. Soures, and C. P. Verdon, Opt. Commun. **133**, 495 (1997).
[24] M. C. Richardson, P. W. McKenty, F. J. Marshall, C. P. Verdon, J. M. Soures, R. L. McCrory, O. Barnouin, R. S. Craxton, J. Delettrez, R. L. Hutchison, P. A. Jaanimagi, R. Keck, T. Kessler, H. Kim, S. A. Letzring, D. M. Roback, W. Seka, S. Skupsky, B. Yaakobi, S. M. Lane, and S. Prussin, in *Laser Interaction and Related Plasma Phenomena*, edited by H. Hora and G. H. Miley (Plenum, New York, 1986), Vol. 7, p. 421.